

## RESEARCH ARTICLE

# Fibrinogen regulates lesion border-forming reactive astrocyte properties after vascular damage

Pasquale Conforti<sup>1,2</sup> | Szilvia Mezey<sup>1</sup> | Suvra Nath<sup>1,2</sup> | Yu-Hsuan Chu<sup>1,2</sup>  |  
Subash C. Malik<sup>1,2</sup> | Jose C. Martínez Santamaría<sup>1,2</sup> | Sachin S. Deshpande<sup>1,2</sup> |  
Lauriane Pous<sup>1,2</sup> | Barbara Zieger<sup>3</sup> | Christian Schachtrup<sup>1,4</sup> 

<sup>1</sup>Faculty of Medicine, Institute of Anatomy and Cell Biology, University of Freiburg, Freiburg, Germany

<sup>2</sup>Faculty of Biology, University of Freiburg, Freiburg, Germany

<sup>3</sup>Department of Pediatrics and Adolescent Medicine, University Medical Center, Freiburg, Germany

<sup>4</sup>Faculty of Medicine, Center for Basics in NeuroModulation (NeuroModulBasics), University of Freiburg, Freiburg, Germany

**Correspondence**

Christian Schachtrup, Institute of Anatomy and Cell Biology, University of Freiburg, Albertstr. 17, 79104 Freiburg, Germany.  
Email: christian.schachtrup@anat.uni-freiburg.de

**Funding information**

Deutsche Forschungsgemeinschaft, Grant/Award Numbers: SCHA 1442/8-1, SCHA 1442/9-1; Else Kröner-Fresenius-Stiftung; European Commission FP7, Grant/Award Number: PIRG08-GA-2010-276989; German Academic Exchange Service Fellowship

**Abstract**

Reactive astrocytes at the border of damaged neuronal tissue organize into a barrier surrounding the fibrotic lesion core, separating this central region of inflammation and fibrosis from healthy tissue. Astrocytes are essential to form the border and for wound repair but interfere with neuronal regeneration. However, the mechanisms driving these astrocytes during central nervous system (CNS) disease are unknown. Here we show that blood-derived fibrinogen is enriched at the interface of lesion border-forming elongated astrocytes after cortical brain injury. Anticoagulant treatment depleting fibrinogen reduces astrocyte reactivity, extracellular matrix deposition and inflammation with no change in the spread of inflammation, whereas inhibiting fibrinogen conversion into fibrin did not significantly alter astrocyte reactivity, but changed the deposition of astrocyte extracellular matrix. RNA sequencing of fluorescence-activated cell sorting-isolated astrocytes of fibrinogen-depleted mice after cortical injury revealed repressed gene expression signatures associated with astrocyte reactivity, extracellular matrix deposition and immune-response regulation, as well as increased gene expression signatures associated with astrocyte metabolism and astrocyte-neuron communication. Systemic pharmacologic depletion of fibrinogen resulted in the absence of elongated, border-forming astrocytes and increased the survival of neurons in the lesion core after cortical injury. These results identify fibrinogen as a critical trigger for lesion border-forming astrocyte properties in CNS disease.

**KEYWORDS**

anticoagulant, blood protein, immune response, neuronal regeneration, reactive astrogliosis, stroke

Pasquale Conforti and Szilvia Mezey contributed equally to this work.

This is an open access article under the terms of the Creative Commons Attribution-NonCommercial-NoDerivs License, which permits use and distribution in any medium, provided the original work is properly cited, the use is non-commercial and no modifications or adaptations are made.

© 2022 The Authors. GLIA published by Wiley Periodicals LLC.

## 1 | INTRODUCTION

Scar formation in the central nervous system (CNS) is often associated with chronic non-resolving pathology that hinders CNS repair (Bradbury & Burnside, 2019; Cregg et al., 2014; Silver & Miller, 2004; Sofroniew, 2018). The CNS lesion comprises two components: the area of focal tissue damage forms a non-neural fibrotic scar (lesion core), composed of stromal-derived fibroblasts and inflammatory cells, and the surrounding penumbra consists of microglial cells and reactive astrocytes (Cregg et al., 2014). Reactive astrocytes are vital for the acute containment of inflammation and prevention of the expansion of inflammatory processes (Bush et al., 1999; Faulkner et al., 2004; Sofroniew, 2005), and scar-forming reactive astrocytes ultimately contribute to the chronic failure of axon regeneration (Cregg et al., 2014; Silver & Miller, 2004). Reactive astrocytes contribute both to beneficial and detrimental elements (Frisen et al., 1995; Ikeda et al., 2001; Lee et al., 1998; Liddelov et al., 2017; Wheeler et al., 2019; Zamanian et al., 2012), and specific aspects of the astrocyte reactivity and scar border-forming astrocyte biology are only poorly understood (Adams & Gallo, 2018; Bradbury & Burnside, 2019; Cohen-Salmon et al., 2021; Escartin et al., 2021; Liu & Chopp, 2016; Sofroniew, 2018). Reactive astrogliosis is characterized by gradual changes in astrocytic morphology, molecular expression profile and cell proliferation with respect to distance from the lesion site. In particular, scar border-forming astrocytes are uniquely positioned precisely at the interface to the non-neural tissue lesion core and change their physiologically defined individual domains in CNS disease (Anderson et al., 2014; Wanner et al., 2013).

Astrocytes become reactive in response to CNS injury and disease characterized by blood-brain barrier (BBB) breakdown or increased vascular permeability, such as in spinal cord injury, Alzheimer's disease, multiple sclerosis, brain trauma and stroke (Burda & Sofroniew, 2014; Pekny et al., 2014; Sofroniew & Vinters, 2010; Wanner et al., 2013). Blood-derived proteins of the coagulation cascade are deposited in the CNS parenchyma and initiate hemostasis and wound repair. However, several aspects of this process are poorly understood, including how blood-derived factors and, in particular, fibrinogen factor into CNS diseases with BBB openings and shape the scar border-forming astrocyte properties and astrocyte-related regeneration processes.

The soluble blood coagulation factor fibrinogen extravasates into the CNS parenchyma upon BBB disruption, is cleaved by thrombin and, upon conversion to insoluble fibrin, serves as a key matrix of blood clots to enable hemostasis (Adams et al., 2004). Many pathological conditions involve vascular disruption and leakage of fibrinogen into the CNS tissue, such as multiple sclerosis, Alzheimer's disease, traumatic brain injury and stroke (Adams, Schachtrup, et al., 2007; Petersen et al., 2018; Pous et al., 2020). Beyond its role in coagulation, fibrinogen acts as a perivascular matrix to directly interact with all cellular components of the neurovascular unit to influence inflammatory, neurodegenerative and repair processes in the injured CNS (Adams, Bauer, et al., 2007; Petersen et al., 2017; Pous et al., 2020; Schachtrup et al., 2007; Schachtrup et al., 2010). Fibrinogen in the

CNS acts as a multi-faceted signaling molecule by interacting with integrin and non-integrin receptors and by functioning as a carrier of growth factors (Adams et al., 2004; Martino et al., 2013; Petersen et al., 2018). Recently, we identified fibrinogen as the primary astrocyte activation signal that promotes the availability of active TGF- $\beta$  after vascular damage (Schachtrup et al., 2010). However, the role of fibrinogen in regulating astrocyte properties contributing to scar border formation remained unknown.

Here, we sought to determine the role of fibrinogen on scar border-forming reactive astrocytes in the telencephalic cortex. Using a mouse model for cortical ischemic stroke (photothrombotic ischemia), we found that fibrinogen deposition is localized in the lesion core and in the lesion rim, directly adjacent to elongated, reactive astrocytes that form the scar border. *Pharmacological depletion of fibrinogen in vivo reduced astrocyte activation, represented by a reduced GFAP expression level, altered extracellular matrix expression and deposition, and decreased inflammation, but caused no change in the spread of inflammation.* Importantly, cells with reactive astrocyte morphology were still present in the penumbra of fibrinogen-depleted animals, but these cells expressed nestin instead of GFAP. A three-dimensional reconstruction of reactive astrocytes revealed a reduced appearance of scar border-forming elongated astroglia with extensive overlapping and interacting processes in fibrinogen-depleted animals. In addition, fibrinogen depletion revealed gene expression signatures associated with immune-response regulation and inhibitory extracellular matrix deposition. Accordingly, fibrinogen depletion increased the number of surviving neurons in the lesion core. Thus, our results show that anti-coagulant fibrinogen-depletion is resulting in beneficiary astrocytes at the scar border.

## 2 | MATERIALS AND METHODS

### 2.1 | Animals

Adult C57BL/6 mice (Charles River) and the *Aldh1l1-EGFP* reporter line (Gong et al., 2003) were used. All animal experiments were approved by the Federal Ministry for Nature, Environment and Consumers Protection of the state of Baden-Württemberg and were performed in accordance with the respective national, federal and institutional regulations.

### 2.2 | Surgery

Photothrombotic ischemia (PT) was performed as described to induce stroke in the cortex of adult mice (Labat-gest & Tomasi, 2013; Pous et al., 2020). Briefly, 15 min after injection of the photosensitive dye Rose Bengal (Sigma-Aldrich; 150 mg/kg body weight, intraperitoneally), a cold light illuminator of 150 W intensity was applied stereotaxically: (Bregma 0; mediolateral [ML],  $-2.4$  mm according to Paxinos and Watson). The region of interest (4 mm diameter) was illuminated for 6 min, and after the light exposure was stopped, the wound was

sutured. To analyze fibrinogen- and fibrin-induced cortical astrocyte scar border formation, mice were depleted of fibrinogen with anicrod as described (Akassoglou et al., 2002; Pous et al., 2020), and fibrinogen conversion into fibrin was inhibited with enoxaparin as described (Stutzmann et al., 2002). Briefly, mice received 2.4 U anicrod, 2.0 mg per kg body weight enoxaparin or control buffer, per day by miniosmotic pumps (0.5  $\mu$ l/h) implanted subcutaneously in their back.

### 2.3 | Histology and immunohistochemistry

Mice were transcardially perfused with ice-cold saline, followed by 4% PFA in phosphate buffer under ketamine and xylazine anesthesia, and brain samples were removed, cryoprotected, embedded in OCT (Tissue-Tek) and frozen on dry ice. Brain samples were cut into 30- or 14- $\mu$ m sections, and immunohistochemistry was performed on coronal brain cryostat sections as described (Schachtrup et al., 2010; Schachtrup et al., 2015). Briefly, sections were permeabilized with PBS-triton 0.1% (14- $\mu$ m-thick sections) or PBS-triton 0.3% (30- $\mu$ m-thick sections) for 30 min, blocked in 5% BSA for 1 h and finally incubated overnight with primary antibody in PBS with 1% BSA. Primary antibodies used were rat anti-CD68 (1:500, Bio-Rad, MCA1957), mouse anti-chondroitin-sulfate proteoglycans (CSPGs)(1:200, Sigma, C8035), rabbit anti-GFAP (1:2000, Abcam, ab7260), rat anti-GFAP (1:2000, Invitrogen, 13-0300), rabbit anti-fibrinogen (1:10000, USBiological, F4203-02C), sheep anti-fibrinogen (1:500, USBiological, F4203-02F), goat anti-Nestin (1:200, Santa Cruz, sc-21,249), goat anti-Nestin (1:500, Antibodies-Online, ABIN188165), rabbit anti-NeuN (1:500, Abcam, ab177487), rabbit anti-S100 $\beta$  (1:2000, Abcam, ab52642), goat anti-IBA-1 (1:500, Abcam, ab5076), rabbit anti-laminin-111 (1:500, Sigma, L9393), Armenian hamster anti-plexin-B2 (1:500, eBioscience, eBio3E7). The ApopTag kit (Merck) was used for the detection of apoptotic cells according to the manufacturer's instructions. Briefly, sections were treated with 10 mM citrate buffer at 95°C for 30 min prior to permeabilization. Before blocking, sections were incubated in ethanol-glacial acetic acid at 4°C for 5 min. Secondary antibodies used included donkey antibodies to rabbit, rat, guinea pig, mouse, sheep and goat conjugated with Alexa Fluor 488, 594 or 405 (1:200, Jackson ImmunoResearch Laboratories). Sections were cover-slipped with Fluoromount (Southern Biotechnology) containing DAPI (Southern Biotechnology) or DraQ5 (Abcam).

### 2.4 | Astrocyte isolation and culture

Cortical astrocytes were isolated as described (Schildge et al., 2013). Brain cortices were isolated at P3 and transferred into HBSS (Invitrogen). The dura mater was removed, and the cortices were minced with scissors. Four cortices were transferred into 21.5 ml of HBSS (Invitrogen), digested in 2.5 ml of trypsin-EDTA (2.5%, Invitrogen) and 1.0 ml of pancreatin (2.5%, ICN Biochemicals) for 30 min at 37°C with occasional shaking. Trypsin was deactivated by adding 7.5 ml of DMEM with 10% fetal bovine serum (Invitrogen) and 1.5%

penicillin/streptomycin (Invitrogen). Digested cortices were collected by centrifugation at 500  $\times$  g for 5 min, resuspended in 20 ml of DMEM with 10% heat-inactivated fetal bovine serum and 1% penicillin/streptomycin, and plated onto poly-*d*-lysine-coated 75-cm<sup>2</sup> tissue culture flasks. The media were changed on day 2 and every third day thereafter. After 10–14 days, when astrocytes had reached confluency, microglia and oligodendrocytes were removed by shaking the flasks at 240 rpm for 6 h. The adherent astrocyte cultures were rinsed with PBS and passaged using trypsin-EDTA (1:3 split). After astrocytes reached confluency, they were used for experiments.

### 2.5 | Fibrinogen and enoxaparin treatment of astrocytes

For astrocyte cell death assays, primary cortical astrocytes were plated on poly-*d*-lysine-coated (Millipore) eight-well culture slides (BD Falcon) at a density of 100,000 cells per well in astrocyte culture medium. Primary astrocytes were treated with hirudin (five International Units, Sigma Aldrich) for 15 min and then with fibrinogen (2.5 mg/ml; Calbiochem) and subsequently cultured for 2 days. To determine the effects of enoxaparin on astrocytes, primary cortical astrocytes were plated on poly-*d*-lysine-coated (Millipore) eight-well culture slides (BD Falcon) at a density of 100,000 cells per well in astrocyte culture medium. Primary astrocytes were treated with 100  $\mu$ g/ml of enoxaparin for the indicated time points. As positive control recombinant human TGF- $\beta$  has been used (20 ng/ml, R&D Systems).

### 2.6 | Immunocytochemistry

Cells were rinsed with ice-cold PBS, fixed in 4% PFA for 30 min at 4°C, washed three times with PBS, permeabilized for 10 min at 4°C in PBS plus 0.1% Triton X-100 (by volume), blocked in PBS with 5% BSA for 30 min at 4°C, and washed three times in PBS. The primary antibodies used were rat anti-GFAP (1:2000, Invitrogen, 13-0300) and rabbit anti-cleaved-caspase 3 (1:1000, Cell Signaling, #9661), and the secondary antibodies used included donkey antibodies to rat, rabbit and mouse conjugated with Alexa Fluor 488, 594 or FITC (1:200, Jackson ImmunoResearch Laboratories).

### 2.7 | Immunoblot

For immunoblotting to detect neurocan in the lesion core of anicrod-treated and control animals 6 days after PT, brain lesion tissue was isolated, digested in lysis buffer and centrifuged for 5 min at 1500 g. Supernatants were removed and tissue was digested for 3 h at 37°C with 0.01 U of chondroitinase ABC enzyme (ChABC) to digest CSPGs. Protein extracts were separated by electrophoresis on a 4%–12% gradient. The following primary antibodies were used: rat anti-neurocan (1:500, Invitrogen, PA5-79718) and rabbit anti-GAPDH (1:1000, Cell

Signaling, #2118). Blots were washed three times with TBS-T, incubated with peroxidase-labeled secondary antibodies (goat anti-rat IgG, Cell Signaling Technology, 1:5000), diluted in 5% nonfat milk in TBS-T for 1 h at room temperature, and washed again, followed by detection with chemiluminescence (ECL, GE Healthcare).

## 2.8 | RNA isolation and quantitative PCR

RNA was isolated from primary astrocytes and quantitative real-time PCR was performed as described (Schachtrup et al., 2015). The following primers were used:

<i>Neurocan</i> :	Fwd 5'-TGCAACCACGGCTAAGCTC-3' Rev 5'-GGGGATAAGCAGGCAATGAC-3'
<i>Syndecan</i> :	Fwd 5'-TTTGCCGTTTCTGATCCTG-3' Rev 5'-TTGCCAAGTCGTAAGTCC-3'
<i>GAPDH</i> :	Fwd 5'-CAAGCCGAGAATGGGA-3' Rev 5'-GGCTCACCCCATTTGAT-3'

## 2.9 | RNA sequencing and transcriptome data analysis

For fluorescence-activated cell sorting (FACS) isolation of astrocytes, mice were deeply anesthetized and transcardially perfused with PBS. Brains were harvested immediately, and a 2-mm<sup>2</sup> coronal section containing the photothrombotic lesion area was sliced with a brain matrix, and the glial scar border was further microdissected under the microscope (Leica MZ10). The dissected tissue was chopped into small pieces using a surgical blade, followed by enzymatic digestion with papain (Worthington, 50 units per mouse brain tissue) in PIPES solution [(120 mM NaCl, 5 mM KCl, 50 mM PIPES [Sigma-Aldrich]), 0.6% glucose, 1 × pen/strep in water, pH adjusted to 7.6] for 10 min at 37°C, and mechanically dissociated into single cells with fire-polished glass Pasteur pipettes after adding ovomucoid (Worthington, 0.14 mg/mouse) and DNase I (Invitrogen, 100 units/mouse). Single cells were collected by centrifugation (176 g, 5 min) and re-suspended in DPBS containing 2% FBS for FACS. Live astrocytes were defined as EGFP+DAPI- cells and sorted into Eppendorf tubes containing RLT buffer (RNeasy micro kit, Qiagen) by MoFlo Astrios (Beckman Coulter) using a 100-µm nozzle at 13.1 psi pressure.

Total RNA from FACS isolated astrocytes was extracted using the RNeasy micro kit (Qiagen) according to the manufacturer's instruction. RNA sequencing and transcriptome data analysis was performed by Novogene (Beijing, China). In brief, the RNA sequencing library was generated using the SMART-Seq v4 Ultra-low Input RNA Kit (Takara Bio), and a paired-end 150 bp sequencing was performed on an Illumina Novaseq 6000 at a depth of 50 million reads per sample. Raw data (raw reads) of fastq format were firstly processed through in-

house perl scripts. Clean data (clean reads) were obtained by removing reads containing adapters, poly-N, and low-quality nucleotides. Index of the reference genome was built using Hisat2 v2.0.5 and paired-end clean reads were aligned to the reference genome using Hisat2 v2.0.5. Differential expression analysis was performed using the DESeq2 (3.12.1). The *p* values were adjusted using the Benjamini and Hochberg method. Genes with adjusted *p* value < .05 and |log<sub>2</sub> (FoldChange)| > 1 were considered as differentially expressed. Gene Ontology (GO) enrichment analysis of differentially expressed genes was implemented using the clusterProfiler R package with the corrected *p* value < .05.

## 2.10 | Morphometric analysis of astrocytes

Immunohistochemistry was performed on coronal brain cryostat sections as described under 2.3. Briefly, 30-µm mouse brain sections were examined with rabbit anti-GFAP primary antibody (1:2000, Abcam), followed by Alexa Fluor 488-conjugated secondary antibody (1:200, Jackson ImmunoResearch Laboratories). Sections were cover-slipped with Fluoromount containing DAPI (Southern Biotechnology). Images were acquired with a Leica TCS SP8 laser confocal microscope with 60× oil immersion objectives. Z-stacks were collected with a 0.5–1.0-µm step size at 1024 × 1024 pixel resolution, and then images were analyzed using the IMARIS software (Bitplane) and further analyzed as previously published with modifications (Erny et al., 2015). 3D reconstruction was performed using IMARIS Filament Tracer with no loops allowed and spot detection mode to determine start and end points of astrocyte process extensions. Although the analysis was performed automatically by the IMARIS software, we separately verified that each astrocyte process originated from one defined cell and manually removed false connections. Additionally, IMARIS Surface Rendering was implemented to render the astrocyte's soma separately. Among the various morphometric parameters that IMARIS automated rendering algorithm provided, just four (surface area and volume of GFAP+ soma, number of branch points of GFAP+ astrocytic processes and surface area of GFAP+ astrocytic processes) were analyzed in detail that enabled us to make comparisons between the different experimental conditions.

## 2.11 | Microscopy and image-acquisition and analysis

Overview images were taken using the 10× objective of a motorized-stage Zeiss AxioImager2 microscope and the Zeiss ZEN software. For colocalization analysis, images from coronal brain sections were acquired with a Leica TCS SP8 laser confocal microscope with 10, 20 and 40× oil immersion objectives. Images were generated from z-stack projections (0.5–1.0 µm step size) through a distance of 15–20 µm per brain section. The colocalization of different markers was analyzed with the LAS AF analysis software by displaying the

z-stacks as maximum intensity projections and using axis clipping and rotation of the 3D-rendered images. For immunoreactivity (IR) analysis, 10–20- $\mu\text{m}$  projection z-stacks were saved as TIFFs. With ImageJ (NIH), the images were converted into black and white 16-bit images and thresholded. Total IR was calculated as percentage area density defined as the number of pixels (positively stained areas) divided by the total number of pixels (sum of positively and negatively stained area) in the imaged field. For colocalization and IR analysis, images were analyzed and averaged on at least three randomly selected brain sections with an area of  $387.5 \times 387.5 \mu\text{m}$  (fibrinogen, GFAP, CSPG, Laminin-111 and IBA-1, Figures 1, 3, 4), with an area of  $100 \times 290 \mu\text{m}$  (Nestin, Figure 6d), with an area of  $100 \times 150 \mu\text{m}$  (Figure S3). For cell-count analysis, images were analyzed on las X, and averaged on at least three randomly selected brain sections with an area of  $100 \times 290 \mu\text{m}$  (S100 $\beta$ , GFAP, Figure 6b), with an area of  $400 \times 400 \mu\text{m}$  at the lesion rim (TUNEL, S100 $\beta$ , Figure S2a), and in the lesion core for neuronal cell-count analysis (NeuN, Figure 8b). For cell-culture assays, images used for quantifications were acquired with an Axioplan 2 Imaging epifluorescence microscope with 20 $\times$  objective and analyzed with the AxioVision image analysis software (Carl Zeiss). The images were saved in TIFF format and quantified with the “Cell counter” plugin of ImageJ. The IR measurements were performed by using ImageJ, as described above.

2.12 | Statistics

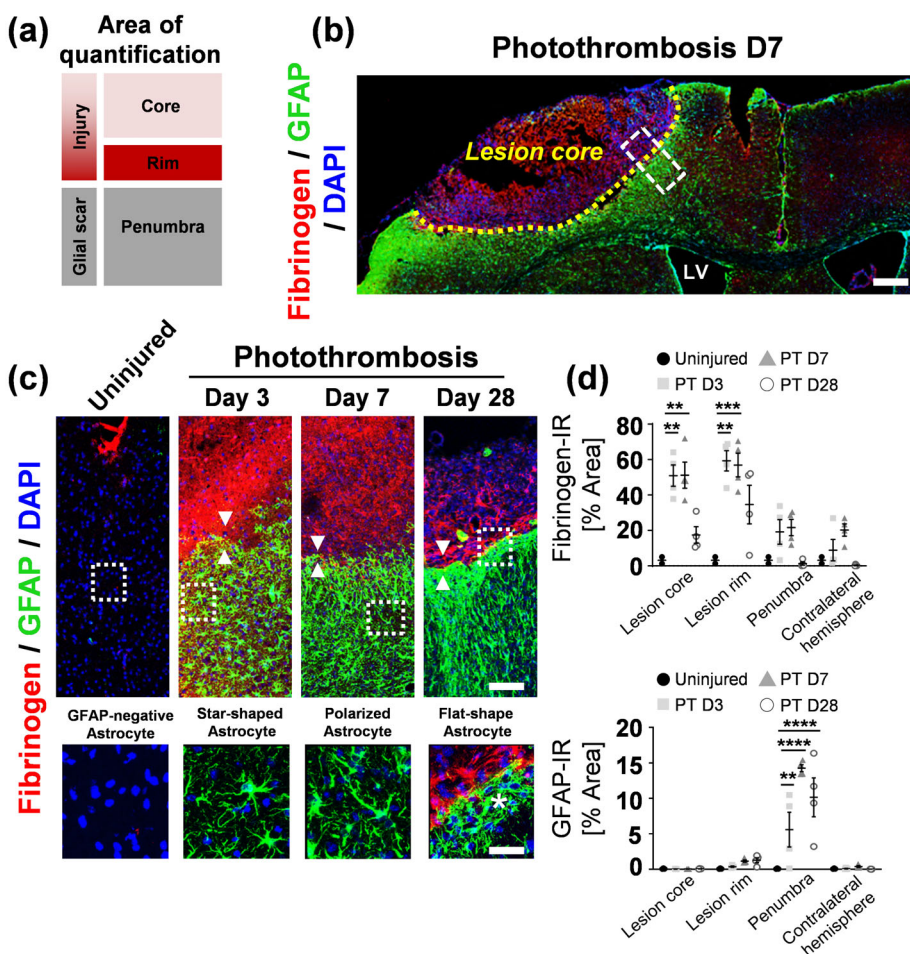
Data are shown as means  $\pm$  SEM. Statistical significance was determined using one-way ANOVA and Bonferroni’s post-test (multiple comparisons) and non-parametric, unpaired Mann–Whitney test. Statistical calculations were performed with GraphPad Prism.

3 | RESULTS

3.1 | Fibrinogen deposition at the interface of scar border-forming reactive astrocytes after cortical brain injury

To identify the role of fibrinogen on astrocytic border formation, we used PT, a mouse model for ischemic stroke that induces a defined cortical lesion with fibrinogen deposition and reactive astrogliosis (Figure 1a,b). At 3 and 7 days after PT, we detected massive fibrin deposition in the lesion core and lesion rim, coinciding with the formation of the astrocyte scar border (Figure 1c,d, enlargement of typical reactive astrocytes at different time points after PT at the bottom). Fibrinogen was not detected in uninjured mice and was present at low, but detectable levels in the contralateral hemisphere of

**FIGURE 1** Fibrinogen deposition at the interface of the forming scar border after cortical injury. (a) Scheme illustrating areas of quantification. (b) Representative image showing immunolabeling for fibrinogen (red) and GFAP (green) in the lesion area (lesion core indicated by yellow dotted line) 7 days after photothrombotic (PT) ischemia. White box indicates the quantification area ( $n = 4$  mice). Scale bar, 500  $\mu\text{m}$ . (c) Immunolabeling for fibrinogen (red) in combination with GFAP (green) 3, 7 and 28 days after PT and uninjured control. Arrowheads indicate fibrinogen deposition adjoining scar border-forming astrocytes. White box indicates typical astrocyte morphology at the fibrinogen–reactive astrocyte interface at different days after PT (bottom, asterisk indicating elongated, scar-border-forming astrocyte). Scale bars, 140  $\mu\text{m}$ , top and 50  $\mu\text{m}$ , bottom. (d) Quantification of fibrinogen and GFAP immunoreactivity (IR) per lesion core, lesion rim, penumbra and contralateral hemisphere at different time points after PT and in uninjured mice.  $N = 4$  mice, mean  $\pm$  SEM, one-way ANOVA and Bonferroni’s multiple comparisons test,  $**p < .01$ ,  $***p < .001$ ,  $****p < .0001$ . LV, lateral ventricle



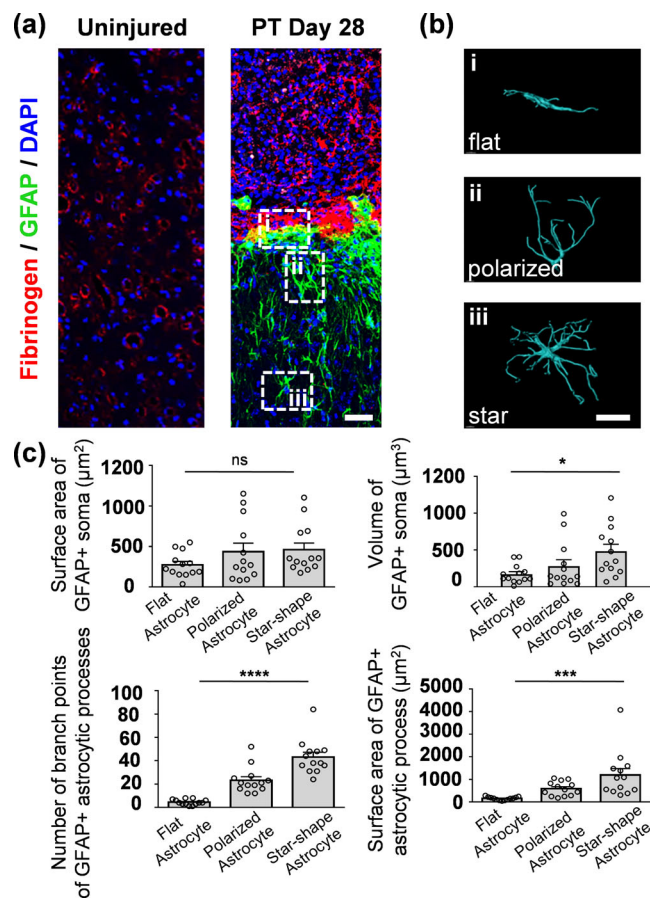


**FIGURE 2** Distinct morphology of reactive astrocytes in relation to distance from the fibrin deposit at the scar border after photothrombotic (PT). (a) Immunolabeling for fibrinogen (red) in combination with GFAP (green) 28 days after PT and uninjured control. White boxes indicating astrocytes with distinct morphology at the scar border (i), inner penumbra (ii) and outer penumbra (iii). Scale bar, 50  $\mu\text{m}$ . (b) Three-dimensional reconstruction (scale bar, 5  $\mu\text{m}$ ), and (c) Imaris-based automatic quantification of cell morphology of GFAP<sup>+</sup> astrocytes in a graded distance to the fibrin deposition at the scar border 28 days after PT.  $n = 7$  mice, 13 cells per condition, 39 cells in total, mean  $\pm$  SEM, one-way ANOVA and Bonferroni's multiple comparisons test, \* $p < .05$ , \*\*\* $p < .001$ , \*\*\*\* $p < .0001$  and ns, not significant

injured mice (Figure 1c,d). Interestingly, fibrin deposition localized at the interface of the lesion rim opposing the scar border formed by reactive astrocytes and markedly persisted up to day 28 after PT (Figure 1c,d, white arrowheads, Figure S1). Furthermore, these fibrin deposits at the lesion rim aligned with elongated, scar border-forming astrocytes that wall off the lesion core from functional neural tissue (Figure 1c, with arrowheads and enlargement at the bottom at day 28 after PT, asterisk indicating elongated scar border astrocyte).

To more precisely define the different morphologies of reactive astrocytes in relation to distance from the fibrin deposit at the scar border, we employed an immunohistochemistry-based three-dimensional (3D) reconstruction using the IMARIS technique of GFAP-positive cells at day 28 after PT (Figure 2a,b). GFAP is a major constituent of astrocyte intermediate filaments and is upregulated in reactive astrocytes. This

increase largely reflects changes in the astrocytic cytoskeleton and particularly morphological changes in individual astrocytes. As expected, after PT, reactive astrocytes revealed a hypertrophic, stellate appearance in the outer penumbra (Figure 2b, iii) and a polarized morphology towards the injury site in the inner penumbra (Figure 2b, ii). In striking contrast, individual reactive astrocytes at the interface to the fibrin deposits at the lesion rim exhibited a distinctive elongated morphology, as recently described (Wanner et al., 2013)(Figure 2b, i). Although fibrin is degraded over time after stroke (Figure 1d), fibrin deposits opposing scar border-forming elongated astrocytes remain 28 days after stroke (Figure 2a, right). Overall, these cells showed a reduced volume of GFAP<sup>+</sup> soma, fewer branch points of GFAP<sup>+</sup> astrocytic processes and a reduced surface area of GFAP<sup>+</sup> astrocytic processes, and they formed a distinct scar border directly adjoined to the fibrinogen rim (Figure 2b,c), suggesting that fibrin deposits affect astrocyte morphology.

### 3.2 | Fibrinogen depletion reduces astrocyte reactivity and CSPG expression after PT

Fibrinogen leaking into the CNS upon BBB disruption serves as an early signal for the induction of astrocyte activation (Schachtrup et al., 2010). However, the effects of fibrinogen on parenchymal astrocytes and astrocyte-related regeneration processes are poorly understood. In CNS disease, such as in stroke (Figure 1), fibrinogen enters the CNS in areas of vascular permeability and is deposited as insoluble fibrin, forming a provisional extracellular matrix for brain repair (Petersen et al., 2018; Schachtrup et al., 2007). To determine whether fibrinogen or fibrin is required for astrocyte reactivity and functions, we treated mice with anicrod to almost completely deplete fibrinogen and fibrin (Schachtrup et al., 2010) or with enoxaparin, a low-molecular-weight heparin that blocks the conversion of fibrinogen into fibrin (Buckley & Sorkin, 1992; Stutzmann et al., 2002).

We then examined the astrocytic expression and extracellular deposition of CSPGs and laminin-111, which are critical for CNS repair processes (Bradbury & Burnside, 2019; Yao et al., 2014). Anicrod-treated animals showed a 93% less fibrinogen from the cortical lesion core than vehicle-treated control animals (Figure 3a,b). Importantly, fibrinogen depletion by anicrod reduced GFAP levels in the lesion rim and in the penumbra by 45%, each (Figure 3a,b), confirming that fibrinogen is necessary for reactive astrocytes (Pous et al., 2020; Schachtrup et al., 2010). Accordingly, fibrinogen depletion by anicrod was accompanied by reduced CSPG expression and deposition in the lesion rim by 56% and penumbra by 47% (Figure 3a,b) and reduced neurocan deposition, a CSPG family member, in the cortical lesion area (Figure 3c). Enoxaparin reduced the fibrinogen deposition, albeit not significantly, in the lesion core by 55%, in the lesion rim by 67% and in the penumbra by 65%. However, increased CSPG expression levels in the lesion core were 90% greater in enoxaparin-treated animals than vehicle-treated control animals, suggesting that soluble fibrinogen and fibrinogen converted to fibrin affect CSPG-producing cells differently (Figure 3a,b). Both, anicrod (66%, lesion core; 71%, lesion rim; 56%, penumbra) and enoxaparin treatment (36% lesion rim) reduced laminin-111 levels. Fibrinogen did not affect

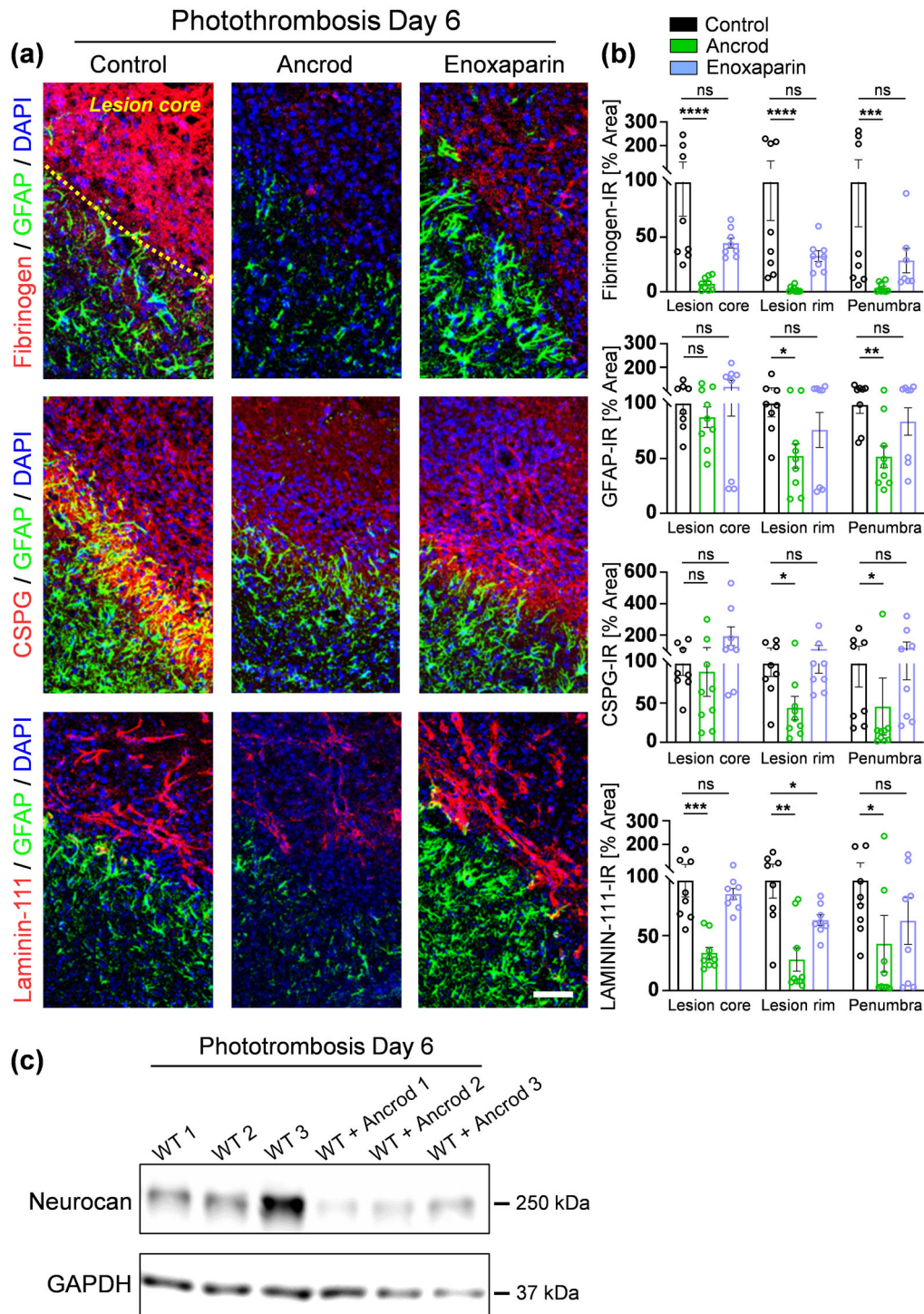


**FIGURE 3** Fibrinogen depletion reduces astrocyte activation and ECM deposition after photothrombotic (PT). (a) Fibrinogen (red, top), chondroitin-sulfate proteoglycans (CSPG) (red, middle) or laminin-111 deposition (red, bottom row) in combination with GFAP+ astrocytes (green) in the brains of fibrinogen-depleted mice (ancrod) and after blocking fibrinogen conversion into fibrin in mice (enoxaparin), compared to control animals (NaCl) at 6 days after PT. yellow dotted line delineates the lesion core. Scale bar, 108  $\mu$ m. (b) Quantifications of fibrinogen, GFAP, CSPG and laminin-111 immunoreactivities (IR) in the different lesion regions.  $N = 8$  mice (NaCl and enoxaparin) and  $n = 9$  (ancrod), mean  $\pm$  SEM, unpaired Mann-Whitney test, \* $p < .05$ , \*\* $p < .01$ , \*\*\* $p < .001$ , \*\*\*\* $p < .0001$  and ns, not significant. (c) Brain lysates of ancrod-treated WT mice show reduced neurocan protein expression, compared to vehicle-treated control mice, 6 days after PT. lysates from three mice per experimental treatment are shown

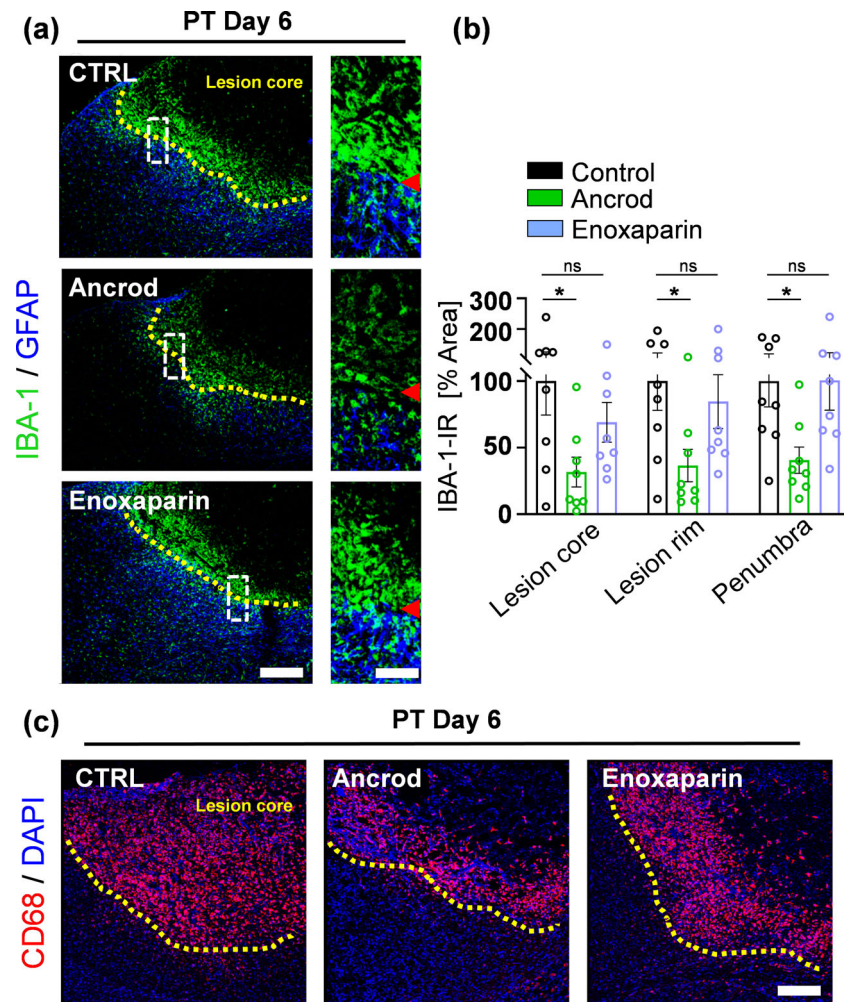


**FIGURE 4** Fibrinogen depletion decreases inflammation in the lesion area after photothrombotic (PT). (a) Immunolabeling for IBA-1 (green) in combination with GFAP<sup>+</sup> astrocytes (blue) in the brain of fibrinogen-depleted mice (ancrod) and after blocking fibrinogen conversion into fibrin in mice (enoxaparin), compared to control animals (NaCl), at 6 days after PT. yellow dotted line delineates the lesion core. Red arrowheads indicate the lesion border. The white boxes indicate the enlargement of the lesion region (right) quantified for IBA-1 immunoreactivity. Scale bars, 250  $\mu$ m; 77  $\mu$ m, enlargement. (b) Quantifications of IBA-1 immunoreactivity (IR) in the lesion area.  $N = 8$  mice, mean  $\pm$  SEM, unpaired Mann-Whitney test,  $*p < .05$  and ns, not significant. (c) Immunolabeling for CD68 (red) in the brains of fibrinogen-depleted mice (ancrod) and after blocking fibrinogen conversion into fibrin in mice (enoxaparin), compared to control animals (NaCl) at 6 days after PT. Scale bar, 250  $\mu$ m. Yellow dotted line delineates the lesion core. Representative images are shown,  $n = 3$  mice

astrocyte cell death *in vivo* or *in vitro* and enoxaparin treatment did not directly regulate astrocyte expression of HSPGs and CSPGs (Figure S2). These data suggest that systemic pharmacologic depletion of fibrinogen by ancrod reduces astrocyte reactivity and extracellular matrix (ECM) deposition and that fibrinogen depletion by ancrod or inhibiting fibrinogen conversion into fibrin by enoxaparin affects astrocyte properties differently.

### 3.3 | Fibrinogen depletion reduces inflammation but does not change the spread of inflammation after PT

Fibrinogen depletion and reduced astrocyte reactivity may alter the spread of inflammation after CNS injury (Bush et al., 1999; Faulkner

et al., 2004). Furthermore, fibrinogen-induced astrocyte activation might affect immune-cell recruitment (Escartin et al., 2019) and fibrin activates microglia (Adams, Bauer, et al., 2007; Ryu et al., 2018). To determine if reduced astrocyte reactivity and altered scar border formation change the inflammatory response and cell spread in pharmacologically fibrinogen-depleted animals after PT, we stained for IBA-1, which is upregulated by activated brain resident microglia and all bone marrow-derived myeloid cells that infiltrate the brain. Interestingly, fibrinogen depletion by ancrod significantly reduced IBA-1<sup>+</sup> myeloid cells in the lesion core, lesion rim and penumbra at 6 days after PT, and blocking fibrinogen conversion into fibrin by enoxaparin slightly reduced IBA-1<sup>+</sup> myeloid cells only in the lesion core (Figure 4a,b). However, fibrinogen depletion did not affect the spread of inflammation (Figure 4a,b, red arrow indicating lesion border, Figure 4c). Reactive astrocytes at the scar border segregate spatially from activated

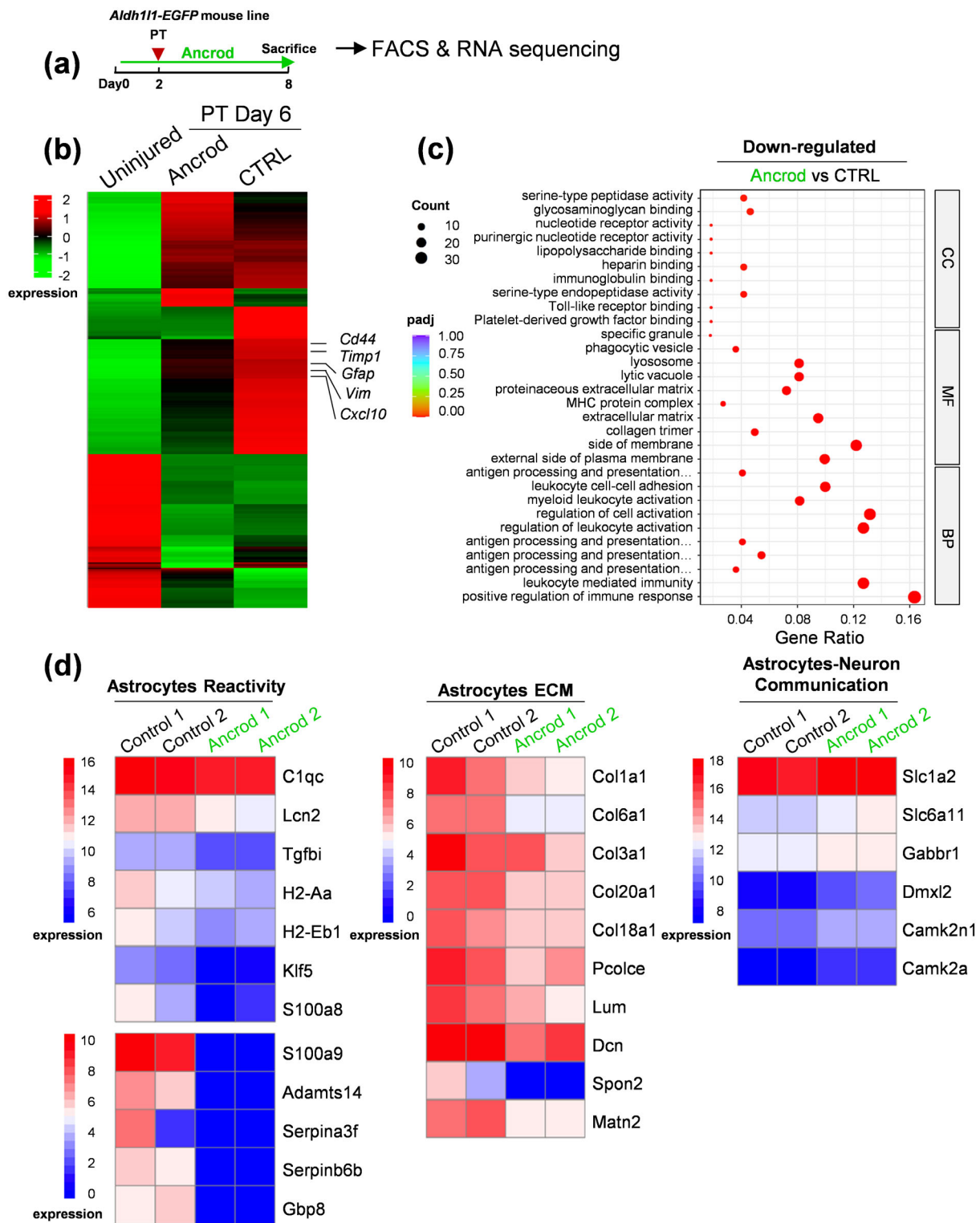


**FIGURE 5** Fibrinogen-induced molecular signature of astrocytes after photothrombotic (PT). (a) Schematic describing the experimental setup for RNA sequencing (RNAseq) on astrocytes isolated by fluorescence-activated cell sorting (FACS) from anicrod-treated and NaCl-treated (control) animals using the *Aldh1l1-yfp* reporter mouse line. (b) Hierarchical clustering of significantly differentially expressed genes (DEGs) from anicrod- and vehicle-treated (control) mice 6 days after PT, compared to uninjured mice. *N* = 2 mice per group. (c) Dot plot showing the top 10 differentially enriched gene ontology (GO) terms of downregulated DEGs, including biological processes (BP), molecular functions (MF) and cell component (CC) in lesion astrocytes of fibrinogen-depleted mice (anicrod), compared to controls (NaCl). (d) Heatmaps of selected astrocyte reactivity-, astrocyte ECM-, and astrocyte-neuronal-related genes

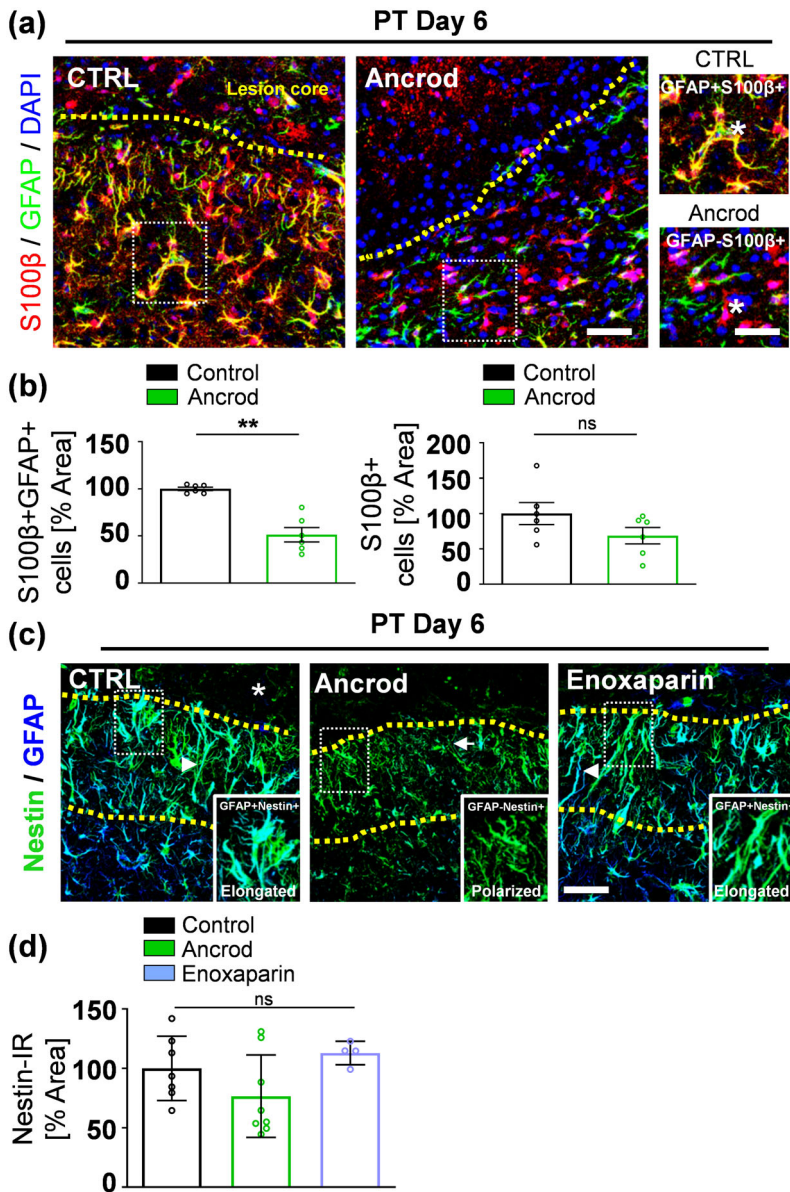


**FIGURE 6** Fibrinogen drives astrocyte properties after photothrombotic (PT). (a) Immunolabeling for S100β (red) in combination with GFAP (green) in the brains of fibrinogen-depleted mice (Ancrod), compared to controls (NaCl), at 6 days after PT. yellow dotted line delineates the lesion core. White boxes indicate enlargements of a S100β + GFAP + (top, asterisk) and a S100β + GFAP- (bottom, asterisk) cell in the lesion area of control and fibrinogen-depleted mice, respectively, 6 days after PT. Scale bars, 45 μm; 40 μm, enlargement. (b) Quantification of S100β + GFAP+ cells and S100β+ cells in the lesion area. N = 6 mice, mean ± SEM, unpaired Mann-Whitney test, \*\*p < .01, ns, not significant. (c) Immunolabeling for nestin (green) with GFAP (blue) in the brain of fibrinogen-depleted mice (Ancrod), compared to controls (NaCl), at 6 days after PT. yellow dotted lines delineate the lesion scar border. White arrowheads indicate elongated, reactive astrocytes (control, left and enoxaparin, right) and the arrow indicates branched astrocytes in fibrinogen-depleted animals (Ancrod, middle). White boxes indicate enlargement of elongated, border-forming reactive astrocytes (control, left and enoxaparin, right) and of branched, polarized astrocytes in fibrinogen-depleted animals (Ancrod, middle). Scale bar: 45 μm. (d) Quantifications of nestin immunoreactivity (IR) in the lesion area. N = 8 mice, mean ± SEM, unpaired Mann-Whitney test, ns, not significant

myeloid cells in the lesion core via injury-induced microglia/macrophages Plexin-B2 expression (Zhou et al., 2020). Importantly, fibrinogen-depletion reduced astrocyte activation and inflammation and also reduced Plexin-B2 levels at the scar border (Figure S3). These data suggest that, although fibrinogen-depletion alters the properties of reactive astrocytes and ECM composition, it preserves their function to limit the spread of inflammation after PT.

### 3.4 | Fibrinogen drives the molecular properties of reactive astrocytes after PT

We next sought to identify the genes in astrocytes regulated by fibrinogen deposition in the lesion area after PT. Using the *Aldh1l1-EGFP* reporter mouse line (Gong et al., 2003), we performed RNA sequencing (RNAseq) on astrocytes from Ancrod-treated and NaCl-treated

(control) animals isolated by fluorescence-activated cell sorting (FACS)(Figure 5a, Figure S4a). As expected, cortical ischemic injury resulted in the upregulation of genes related to astrocyte reactivity (e.g., *Gfap*, *Vim*, *Timp1*, *Cd44* and *Cxcl10*) in vehicle-treated control mice 6 days after PT (Figure 5b). Importantly, fibrinogen depletion by Ancrod drastically changed the overall gene expression profile of reactive astrocytes, compared to vehicle-treated controls 6 days after PT (Figure S4b, complete list of differently regulated genes [DEGs] in Table S1). We analyzed the fibrinogen-regulated genes by Gene Ontology (GO) classification. The categorization by cell component (CC), molecular functions (MF) and biological processes (BP) revealed a down-regulation of the GO categories related to “cell activation” and “immune response” as well as “extracellular matrix” and “ECM binding” in fibrinogen-depleted mice, suggesting that fibrinogen drives scar-border forming astrocyte reactivity and properties in the cortical lesion area (Figure 5c). Accordingly, levels of several core genes

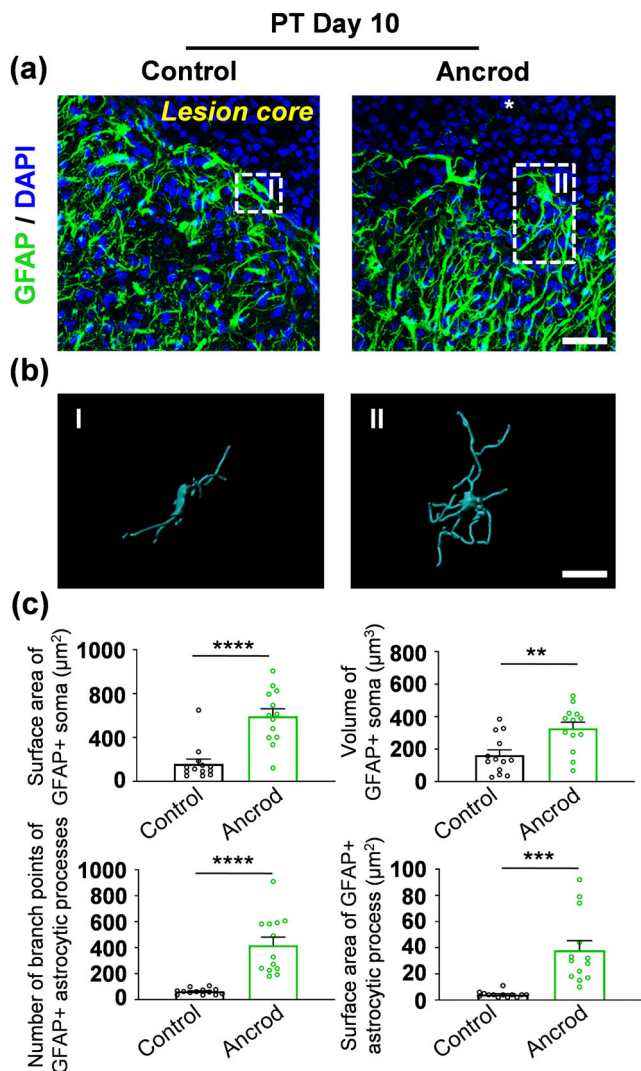


**FIGURE 7** Absence of scar-border-forming reactive astrocytes after fibrinogen depletion. (a) Immunolabeling for GFAP (green) in combination with DAPI (blue) in the brains of fibrinogen-depleted mice (ancrod), compared to controls (NaCl), at 10 days after photothrombotic (PT) (scale bar, 30  $\mu\text{m}$ ). White boxes indicate astrocyte morphology at the scar border.  $N = 4$  mice. (b) Three-dimensional reconstruction (scale bar, 6  $\mu\text{m}$ ), and (c) Imaris-based automatic quantification indicates cell morphology of GFAP+ astrocytes at the scar border 10 days after PT.  $n = 4$  mice, 13 cells per condition, mean  $\pm$  SEM, unpaired Mann-Whitney test,  $**p < .01$ ,  $***p < .001$ ,  $****p < .0001$

indicating astrocyte reactivity after stroke (Zamanian et al., 2012), such as *Lcn2*, *S100a9*, and *Serpina3f*, were lower in ancrod-treated mice than vehicle-treated control mice (Figure 5d, left). Importantly, in line with our data on reduced CSPGs (Figure 3), several genes associated with the inhibitory ECM at the scar border (e.g., *Col1a1*, *Col6a1*, *Col20a1*, *Dcn*, *Lum*, and *Spon2*), were down-regulated in fibrinogen-depleted animals 6 days after PT, suggesting that fibrinogen is a major inducer of astrocyte-derived inhibitory ECM composition at the scar border.

Astrocytes play an active role in the energy metabolism of the diseased brain (Belanger et al., 2011; Sofroniew, 2009), and fibrinogen

depletion upregulates GO categories associated with higher energy metabolism and increased ATP synthesis (Figure S4). In addition, expression of genes related to astrocyte-neuron communication (e.g., *Camk2a*, *Dmxl2*, *Gabbr1* and *Slc1a2*) was increased in ancrod-treated animals, suggesting that fibrinogen-depletion supports astrocyte metabolism and astrocyte-mediated neuronal functions (Figure 5d, right and Figure S4).

### 3.5 | Fibrinogen depletion inhibits astrocyte transformation into scar border-forming elongated cells

Next, we tested how fibrinogen alters the morphological properties of reactive astrocytes after PT. Pharmacological depletion of fibrinogen strongly reduced GFAP expression and inflammation without boosting the spread of inflammatory cells, suggesting that fibrinogen determines diverse astrocytic properties (Figures 1–5). To determine if reactive astrocytes with altered molecular properties occur in fibrinogen-depleted animals, we also used the markers S100 $\beta$ , which labels both non-reactive and activated astrocytes, and nestin, which is re-expressed in reactive astrocytes (Gotz et al., 2015). Fibrinogen depleted animals had 50% fewer GFAP+S100 $\beta$ + cells than controls, as expected (Figure 6a,b), indicating fewer GFAP+ classical, reactive astrocytes. Surprisingly, fibrinogen depletion did not significantly alter the number of S100 $\beta$ + cells (Figure 6a,b) or of Nestin+ cells, compared to controls (Figure 6c,d). After CNS injury, astrocytes proliferate adjacent to the vasculature and are a major source for the formation of the glial scar border. However, depletion of fibrinogen did not affect the proliferation and formation of new (Ki67+/EdU+) local, perivascular astrocytes at the lesion site (Pous et al., 2020), suggesting that fibrinogen deposition does not affect the overall astrocyte cell number in the lesion area, but these cells expressed S100 $\beta$  or nestin instead of GFAP (Figure 6). Importantly, fibrinogen depletion with ancrod resulted in a lack of elongated, flat astrocytes that form the compact scar border, whereas astrocytes with processes polarized towards the lesion area were still present (Figure 6c, middle, inset). Blocking fibrinogen conversion into fibrin by enoxaparin did not significantly alter the number of Nestin+ cells or the morphology of astrocytes at the scar border (Figure 6c, right, Figure 6d). These data suggest that fibrinogen deposition at the lesion border affects scar border-forming astrocyte morphology and function. To precisely define the morphology of astrocytes forming the scar border at the fibrinogen-astrocyte interface, we examined the morphological profiles of single astrocytes at day 10 after PT, when the flat, elongated morphology of scar border-forming astrocytes is fully established (Figure 7). Detailed analysis of single cells at the scar border, using the imaging program IMARIS, showed an increase in the surface area of GFAP+ soma, volume of GFAP+ soma, number of branch points of GFAP+ astrocytic processes and surface area of GFAP+ astrocytic process in fibrinogen-depleted animals 10 days after PT (Figure 7b,c), compared to palisading, elongated astrocytes along the glial scar border in control animals.

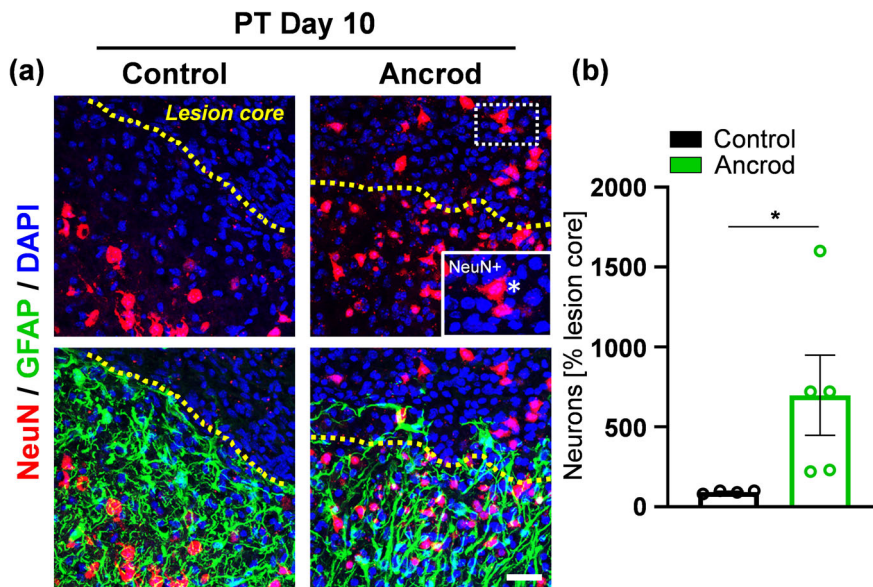


**FIGURE 8** Fibrinogen depletion increases the number of neurons in the lesion core after photothrombotic (PT). (a) Immunolabeling for NeuN (red) in combination with GFAP (green) in the brains of fibrinogen-depleted mice (ancrod), compared to controls (NaCl), at 10 days after PT. yellow dotted line delineates the lesion core. White box indicating NeuN+ neuron in the lesion core of fibrinogen-depleted animals.  $N = 5$  mice. Scale bar, 30  $\mu\text{m}$ . (b) Quantifications of NeuN+ cells in the lesion core.  $N = 5$  mice, mean  $\pm$  SEM, unpaired Mann-Whitney test,  $*p < .05$

### 3.6 | Fibrinogen-depletion increases neuronal survival in the lesion core after PT

Our data showed that fibrinogen alters the molecular and morphological properties of scar border-forming astrocytes after PT. Finally, we investigated whether fibrinogen-regulated astrocyte scar border formation and properties influence repair promoting processes by investigating neuronal cell survival in the non-neural lesion core (Liu & Chopp, 2016; O'Shea et al., 2017). Remarkably, immunolabeling of NeuN+ cells in the lesion core revealed  $\sim 7.5$ -times more neurons in fibrinogen-depleted animals than controls 10 days after PT (Figure 8), suggesting that fibrinogen is critical in astrocyte scar border formation and astrocyte properties impairing regenerative processes after PT.

## 4 | DISCUSSION

In this study, we define how the blood-derived coagulation factor fibrinogen orchestrates glial scar border formation. Our results suggest the following working model in CNS disease. (i) CNS injury and disease associated with a compromised BBB allows fibrinogen to leak into the CNS. Indeed, massive fibrin deposits in the lesion core and rim adjoin scar border-forming reactive astrocytes after cortical brain injury (Figure 9). (ii) Anticoagulant treatment with ancrod (depleting fibrinogen and fibrin) prevents the formation of palisading scar border-forming astrocytes in mice, whereas anticoagulant treatment with enoxaparin (inhibiting fibrinogen conversion into fibrin) does only marginally affect astrocyte reactivity and ECM expression. Depletion of fibrinogen and fibrin reduces astrocyte reactivity, CSPG deposition, neuronal cell death and inflammation with no change in the spread of inflammation. (iii) Anticoagulant treatment with ancrod identified a fibrinogen-induced astrocytic molecular profile, associated with astrocyte reactivity, ECM expression and signaling, and immune response regulation. Deposition of fibrinogen and fibrin at the lesion border

orchestrates astrocyte polarization, ECM composition and the immune cell status (Figure 9). Thus, fibrinogen serves as a critical trigger of scar border-forming elongated astrocyte properties after cortical brain injury.

Breakdown of the BBB and leakage of blood proteins into the CNS parenchyma are key events in glial scar formation. We found that immediate fibrin deposition in the lesion core and rim, is serving as an early signal for the induction of glial scar formation, as previously shown by our group (Schachtrup et al., 2010). Interestingly, in addition to the immediate fibrin deposition due to vascular rupture after stroke, we observed fibrinogen at later times at the lesion rim adjoining the scar border-forming palisading astrocytes. Thus, prolonged BBB opening and fibrinogen leakage at the lesion rim might be involved in a highly dynamic, long-term remodeling processes at the lesion border, affecting potentially both adverse and beneficial astrocytic activities during the repair process (Sofroniew, 2005). Therefore, fibrinogen might orchestrate lesion border characteristics via its immediate and recurrent deposition after injury and in disease, such as SCI (Schachtrup et al., 2007), MS (Adams, Bauer, et al., 2007; Ryu et al., 2018), ischemia-hypoxia (Adhami et al., 2006), stroke (Pous et al., 2020) and Alzheimer's disease (Paul et al., 2007; Ryu & McLarnon, 2009).

Newly formed, elongated and polarized astroglia with extensive overlapping and interacting processes form compact scar borders and interfere with axonal growth, but are also essential for wound repair (Cregg et al., 2014; Silver & Miller, 2004; Sofroniew, 2005). Reactive astrocytes express and secrete inhibitory CSPGs (Cregg et al., 2014; Schachtrup et al., 2010; Schachtrup et al., 2011). Interestingly, while complete fibrinogen and fibrin depletion decreased CSPG secretion, soluble fibrinogen alone, after enoxaparin treatment, resulted in increased CSPG deposition in the lesion core, suggesting that fibrinogen and fibrin differentially regulate astrocytic functions that affect neuronal regeneration. Notably, while fibrinogen-depletion by ancrod reduced the astrocyte reactivity (Figure 3a,b, Figures 5, 6) and CSPG

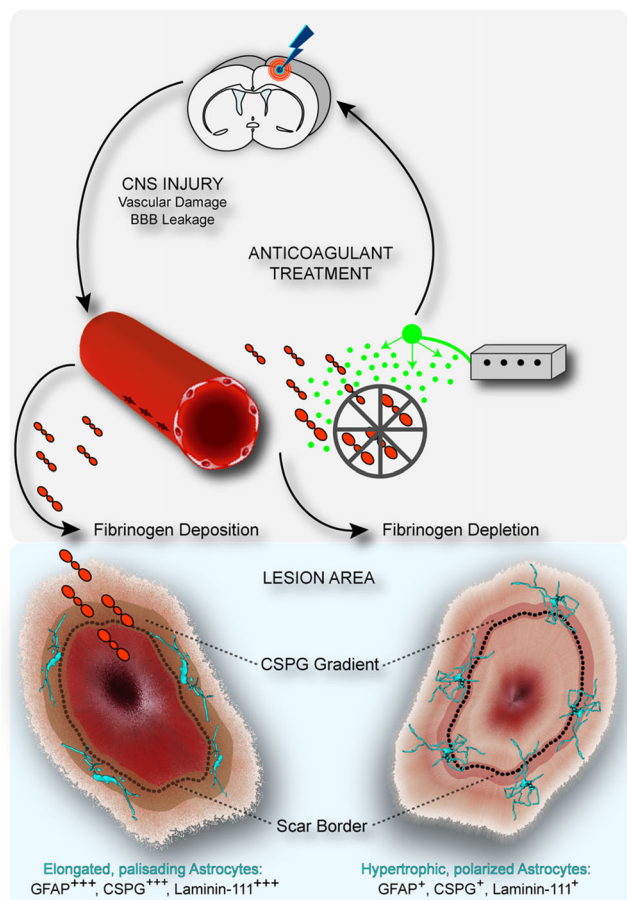


**FIGURE 9** Working model for the role of fibrinogen on border-forming reactive astrocytes in central nervous system (CNS) disease. In the healthy brain, fibrinogen is absent from the CNS due to the intact blood–brain barrier (BBB). BBB disruption or vascular rupture in CNS injury or disease leads to long-lasting fibrinogen deposition along the forming scar border. Fibrinogen deposition modulates the scar-border-forming astrocyte morphology and their properties. Anticoagulant treatment depletes fibrinogen and affects astrocyte scar border-formation with an absence of elongated, palisading astrocytes, reduced extracellular matrix deposition and inflammation, and with an increased neuronal survival. Therefore, fibrinogen matrix deposition might be involved in the highly dynamic remodeling processes at the lesion border orchestrating the regeneration process

neurocan core protein expression and deposition in the lesion area (Figure 3c), we cannot rule out that fibrinogen-depletion alters CSPG modifications to affect its immunoreactivity and, thus, labeling intensity might not correlate with core protein expression levels of particular CSPG family members. Anticoagulant treatments affect the CSPG matrix and influence the repair-promoting laminin-111 expression and secretion (Yao et al., 2014), suggesting that fibrinogen and its converted form fibrin regulate the morphology and properties of scar border-forming astrocytes in addition to their function in triggering astrocyte scar formation (Schachtrup et al., 2010). Importantly, anticoagulant treatment with anicrod revealed a fibrinogen-induced astrocyte gene expression signature, placing fibrinogen at the nexus of astrocyte reactivity, scar border

formation, ECM composition and immune cell response in the lesion area.

The scar border separates neurotoxic non-neural tissue in the lesion core from healthy CNS parenchyma and has been largely attributed to a high concentration of inhibitory proteins, including CSPGs and collagens. We found that fibrinogen depletion changed the astrocyte morphology and functionality. Also, fibrinogen depletion specifically prevented the formation of palisading, scar border-forming astrocytes and drastically reduced the expression and secretion of CSPGs, such as Neurocan. However, hypertrophic, polarized astrocytes could still fulfill the function in preventing the spread of neurotoxic inflammation. Future studies will further elucidate how fibrinogen deposition in the lesion environment affects the individual astrocyte types and if fibrinogen triggers inhibitory rather than beneficial astrocyte properties. Pharmacologic fibrinogen depletion changed the astrocyte gene expression profile associated with increased astrocyte metabolism and astrocyte-neuron communication and reduced inhibitory ECM expression. It also increased neuronal survival in the lesion core, suggesting that pharmacological depletion of an excess of fibrinogen may be of clinical interest for treating neurological diseases with chronic or repeated opening of the BBB and associated scar formation.

Molecular cues coordinating astrocyte scar border-formation and astrocytic properties in CNS disease are poorly described. Fibrinogen regulates astrocyte morphology and properties affecting scar border-formation (this study), and our previous data showed that fibrinogen triggers astrocyte scar formation (Schachtrup et al., 2010). Astrocyte scar border-formation depends on STAT-3 (Okada et al., 2006; Wanner et al., 2013). Selective deletion of STAT-3 from astrocytes disrupted the organization into dense mesh-like arrangements, resulting in increased spread of inflammation and decreased neuronal survival. This study shows that fibrinogen depletion disrupted the formation of scar border palisading astrocytes with decreased inflammation and improved neuronal survival. In addition, we found that fibrinogen regulates plexin-B2 expression by myeloid cells and collagen gene expression by astrocytes, potentially altering the ECM compaction and corralling at the scar border (Hara et al., 2017; Zhou et al., 2020). Our previous study revealed that fibrinogen triggers astrocyte scar formation via TGF-beta signaling (Schachtrup et al., 2010). The STAT and Smad signaling pathways cooperate to induce GFAP expression and astrogenesis (Nakashima et al., 1999). Future studies will determine if fibrinogen regulates the morphology and properties of astrocyte scar border cells and their ECM expression exclusively via the Smad signaling pathways, in cooperation with STAT signaling, or by means of a signaling pathway yet to be defined.

Fibrinogen, as the major component of blood clots, is an essential component of the coagulation system that maintains hemostasis (Holmback et al., 1996; Rooney et al., 1996). Patients lacking fibrinogen, a disorder termed afibrinogenemia, have severe bleeding complications (Litvinov & Weisel, 2016). However, the fibrin network might also orchestrate the wound-healing process by promoting inflammation to remove damaged tissue and by initiating glial scar formation to



separate the lesion core from intact tissue. Indeed, we found that fibrinogen depletion affects both: the lesion core had fewer inflammatory cells but more surviving neurons and astrocytes in the surrounding scar border and penumbra had altered morphology and functionality. Thus, anticoagulants that effectively reduce fibrinogen and fibrin formation, while still ensuring hemostasis, may be of clinical interest for treating neurological diseases with chronic or repeated opening of the BBB. Interestingly, our study showed that enoxaparin, a low-molecular-weight heparin in daily clinical use, affects astrocyte properties. However, hemorrhagic complications of fibrin depletion may complicate widespread clinical use of anticoagulant reagents for chronic CNS disease. The cortical lesion area after PT contains resident and locally produced reactive astrocytes, as well as SVZ-derived newborn astrocytes (Bardehle et al., 2013; Benner et al., 2013; Bohrer et al., 2015; Faiz et al., 2015; Wanner et al., 2013), with both beneficial and inhibitory roles in brain injury (Bardehle et al., 2013; Burda et al., 2015; Cregg et al., 2014; Silver & Miller, 2004). Fibrinogen triggers astrocyte reactivity by promoting the availability of active TGF-beta (Schachtrup et al., 2010), regulates astrocyte scar border formation and astrocyte functionality (this study), and provokes astrocyte differentiation from NSPCs via BMP receptor signaling (Pous et al., 2020). Our study suggests that manipulation of fibrinogen-induced signaling pathways in astrocytes could control their fate and functions in ways tailored to promote CNS repair.

In conclusion, we report that fibrinogen regulates astrocyte reactivity, inhibitory ECM deposition and astrocyte-immune interactions, suggesting that excess and prolonged fibrinogen and fibrin deposition establish an inhibitory environment with a robust glial scar border formation. Future studies will determine how fibrinogen affects specific astrocyte and other lesion area cell populations and their interaction in different CNS injuries and diseases. Our findings represent a critical step forward for testing the fibrinogen reduction (anticoagulant therapy) or manipulation of fibrinogen-induced signaling pathways in astrocytes for improving regeneration. They suggest a novel therapeutic strategy via manipulating fibrinogen-astrocyte interaction for reducing astrocytic scar border formation with reduced inhibitory ECM deposition and inflammation, which might improve functional outcomes in several CNS injuries and diseases, such as brain trauma, spinal cord injury as well as in stroke.

## ACKNOWLEDGMENTS

We thank Meike Ast-Dumbach for outstanding technical assistance, Mark D. Eyre and Gary Howard for language editing, Andreas Schober for graphics, and the University of Freiburg Live Imaging Center (LIC) for microscopy support. This study was supported by the German Academic Exchange Service Fellowship to S.C.M., the European Commission FP7 Grant PIRG08-GA-2010-276989, the Else Kröner-Fresenius-Stiftungs Grant, and the German Research Foundation Grants SCHA 1442/8-1 and 1442/9-1 to C.S.

## CONFLICT OF INTEREST

The authors declare no potential conflict of interest.

## AUTHOR CONTRIBUTIONS

*Performed the majority of the experiments and analyzed data:* Pasquale Conforti and Szilvia Mezey. *Performed surgeries:* Sachin S. Deshpande and Lauriane Pous. *Contributed to histology, immunocytochemistry and biochemical experiments:* Suvra Nath, Yu-Hsuan Chu, Subash C. Malik, and Jose C. Martínez Santamaría. *Provided crucial reagents and contributed to the experimental design:* Barbara Zieger. *Designed the study, analyzed data, coordinated the experimental work and wrote the manuscript with contributions from all authors:* Christian Schachtrup.

## DATA AVAILABILITY STATEMENT

The data that support the findings of this study are available from the corresponding author upon reasonable request.

## ORCID

Yu-Hsuan Chu <https://orcid.org/0000-0002-7594-321X>

Christian Schachtrup <https://orcid.org/0000-0001-9851-6299>

## REFERENCES

- Adams, K. L., & Gallo, V. (2018). The diversity and disparity of the glial scar. *Nature Neuroscience*, 21(1), 9–15. <https://doi.org/10.1038/s41593-017-0033-9>
- Adams, R. A., Bauer, J., Flick, M. J., Sikorski, S. L., Nuriel, T., Lassmann, H., Degen, J. L., & Akassoglou, K. (2007). The fibrin-derived gamma377-395 peptide inhibits microglia activation and suppresses relapsing paralysis in central nervous system autoimmune disease. *The Journal of Experimental Medicine*, 204(3), 571–582.
- Adams, R. A., Passino, M., Sachs, B. D., Nuriel, T., & Akassoglou, K. (2004). Fibrin mechanisms and functions in nervous system pathology. *Molecular Interventions*, 4(3), 163–176.
- Adams, R. A., Schachtrup, C., Davalos, D., Tsigelny, I., & Akassoglou, K. (2007). Fibrinogen signal transduction as a mediator and therapeutic target in inflammation: Lessons from multiple sclerosis. *Current Medicinal Chemistry*, 14(27), 2925–2936.
- Adhami, F., Liao, G., Morozov, Y. M., Schloemer, A., Schmithorst, V. J., Lorenz, J. N., Dunn, R. S., Vorhees, C. V., Wills-Karp, M., Degen, J. L., Davis, R. J., Mizushima, N., Rakic, P., Dardzinski, B. J., Holland, S. K., Sharp, F. R., & Kuan, C. Y. (2006). Cerebral ischemia-hypoxia induces intravascular coagulation and autophagy. *The American Journal of Pathology*, 169(2), 566–583.
- Akassoglou, K., Yu, W. M., Akpınar, P., & Strickland, S. (2002). Fibrin inhibits peripheral nerve remyelination by regulating Schwann cell differentiation. *Neuron*, 33(6), 861–875.
- Anderson, M. A., Ao, Y., & Sofroniew, M. V. (2014). Heterogeneity of reactive astrocytes. *Neuroscience Letters*, 565, 23–29.
- Bardehle, S., Kruger, M., Buggenthin, F., Schwausch, J., Ninkovic, J., Clevers, H., Snippert, H. J., Theis, F. J., Meyer-Luehmann, M., Bechmann, I., Dimou, L., & Gotz, M. (2013). Live imaging of astrocyte responses to acute injury reveals selective juxtavascular proliferation. *Nature Neuroscience*, 16(5), 580–586.
- Belanger, M., Allaman, I., & Magistretti, P. J. (2011). Brain energy metabolism: Focus on astrocyte-neuron metabolic cooperation. *Cell Metabolism*, 14(6), 724–738. <https://doi.org/10.1016/j.cmet.2011.08.016>
- Benner, E. J., Luciano, D., Jo, R., Abdi, K., Paez-Gonzalez, P., Sheng, H., Warner, D. S., Liu, C., Eroglu, C., & Kuo, C. T. (2013). Protective astrogenesis from the SVZ niche after injury is controlled by notch modulator Thbs4. *Nature*, 497(7449), 369–373.
- Bohrer, C., Pfurr, S., Mammadzada, K., Schildge, S., Plappert, L., Hils, M., Pous, L., Rauch, K. S., Dumit, V. I., Pfeifer, D., Dengjel, J., Kirsch, M., Schachtrup, K., & Schachtrup, C. (2015). The balance of Id3 and E47

- determines neural stem/precursor cell differentiation into astrocytes. *The EMBO Journal*, 34(22), 2804–2819. <https://doi.org/10.15252/embj.201591118>
- Bradbury, E. J., & Burnside, E. R. (2019). Moving beyond the glial scar for spinal cord repair. *Nature Communications*, 10(1), 3879. <https://doi.org/10.1038/s41467-019-11707-7>
- Buckley, M. M., & Sorkin, E. M. (1992). Enoxaparin. A review of its pharmacology and clinical applications in the prevention and treatment of thromboembolic disorders. *Drugs*, 44(3), 465–497. <https://doi.org/10.2165/00003495-199244030-00010>
- Burda, J. E., Bernstein, A. M., & Sofroniew, M. V. (2015). Astrocyte roles in traumatic brain injury. *Experimental Neurology*, 275(3), 305–315.
- Burda, J. E., & Sofroniew, M. V. (2014). Reactive gliosis and the multicellular response to CNS damage and disease. *Neuron*, 81(2), 229–248. <https://doi.org/10.1016/j.neuron.2013.12.034>
- Bush, T. G., Puvanachandra, N., Horner, C. H., Polito, A., Ostenfeld, T., Svendsen, C. N., Mucke, L., Johnson, M. H., & Sofroniew, M. V. (1999). Leukocyte infiltration, neuronal degeneration, and neurite outgrowth after ablation of scar-forming, reactive astrocytes in adult transgenic mice. *Neuron*, 23(2), 297–308. [https://doi.org/10.1016/s0896-6273\(00\)80781-3](https://doi.org/10.1016/s0896-6273(00)80781-3)
- Cohen-Salmon, M., Slaoui, L., Mazare, N., Gilbert, A., Oudart, M., Alvear-Perez, R., Elorza-Vidal, X., Chever, O., & Boulay, A. C. (2021). Astrocytes in the regulation of cerebrovascular functions. *Glia*, 69(4), 817–841. <https://doi.org/10.1002/glia.23924>
- Cregg, J. M., DePaul, M. A., Filous, A. R., Lang, B. T., Tran, A., & Silver, J. (2014). Functional regeneration beyond the glial scar. *Experimental Neurology*, 253, 197–207.
- Erny, D., Hrabe de Angelis, A. L., Jaitin, D., Wieghofer, P., Staszewski, O., David, E., Keren-Shaul, H., Mhlahkoiv, T., Jakobshagen, K., Buch, T., Schwierzeck, V., Utermöhlen, O., Chun, E., Garrett, S. W., McCoy, D. K., Diefenbach, D., Staeheli, P., Stecher, B., Amit, I., & Prinz, M. (2015). Host microbiota constantly control maturation and function of microglia in the CNS. *Nature Neuroscience*, 18(7), 965–977. <https://doi.org/10.1038/nn.4030>
- Escartin, C., Galea, E., Lakatos, A., O'Callaghan, J. P., Petzold, G. C., Serrano-Pozo, A., Steinhäuser, C., Volterra, A., Carmignoto, G., Agarwal, A., Allen, N. J., Araque, A., Barbeito, L., Barzilai, A., Bergles, D. E., Bonvento, G., Butt, A. M., Chen, W. T., Cohen-Salmon, M., & Verkhratsky, A. (2021). Reactive astrocyte nomenclature, definitions, and future directions. *Nature Neuroscience*, 24(3), 312–325. <https://doi.org/10.1038/s41593-020-00783-4>
- Escartin, C., Guillemaud, O., & Carrillo-de Sauvage, M. A. (2019). Questions and (some) answers on reactive astrocytes. *Glia*, 67(12), 2221–2247. <https://doi.org/10.1002/glia.23687>
- Faiz, M., Sachewsky, N., Gascon, S., Bang, K. W., Morshead, C. M., & Nagy, A. (2015). Adult neural stem cells from the subventricular zone give rise to reactive astrocytes in the cortex after stroke. *Cell Stem Cell*, 17(5), 624–634. <https://doi.org/10.1016/j.stem.2015.08.002>
- Faulkner, J. R., Herrmann, J. E., Woo, M. J., Tansey, K. E., Doan, N. B., & Sofroniew, M. V. (2004). Reactive astrocytes protect tissue and preserve function after spinal cord injury. *The Journal of Neuroscience*, 24(9), 2143–2155.
- Frisén, J., Haegerstrand, A., Risling, M., Fried, K., Johansson, C. B., Hammarberg, H., Elde, R., Hökfelt, T., & Cullheim, S. (1995). Spinal axons in central nervous system scar tissue are closely related to laminin-immunoreactive astrocytes. *Neuroscience*, 65(1), 293–304.
- Gong, S., Zheng, C., Doughty, M. L., Losos, K., Didkovsky, N., Schambra, U. B., Nowak, N. J., Joyner, A., Leblanc, G., Hatten, M. E., & Heintz, N. (2003). A gene expression atlas of the central nervous system based on bacterial artificial chromosomes. *Nature*, 425(6961), 917–925. <https://doi.org/10.1038/nature02033>
- Gotz, M., Sirko, S., Beckers, J., & Irmeler, M. (2015). Reactive astrocytes as neural stem or progenitor cells: In vivo lineage, in vitro potential, and genome-wide expression analysis. *Glia*, 63(8), 1452–1468. <https://doi.org/10.1002/glia.22850>
- Hara, M., Kobayakawa, K., Ohkawa, Y., Kumamaru, H., Yokota, K., Saito, T., Kijima, K., Yoshizaki, S., Harimaya, K., Nakashima, Y., & Okada, S. (2017). Interaction of reactive astrocytes with type I collagen induces astrocytic scar formation through the integrin-N-cadherin pathway after spinal cord injury. *Nature Medicine*, 23(7), 818–828. <https://doi.org/10.1038/nm.4354>
- Holmback, K., Danton, M. J., Suh, T. T., Daugherty, C. C., & Degen, J. L. (1996). Impaired platelet aggregation and sustained bleeding in mice lacking the fibrinogen motif bound by integrin alpha IIb beta 3. *The EMBO Journal*, 15(21), 5760–5771.
- Ikeda, O., Murakami, M., Ino, H., Yamazaki, M., Nemoto, T., Koda, M., Nakayama, C., & Moriya, H. (2001). Acute up-regulation of brain-derived neurotrophic factor expression resulting from experimentally induced injury in the rat spinal cord. *Acta Neuropathologica*, 102(3), 239–245.
- Labat-gest, V., & Tomasi, S. (2013). Photothrombotic ischemia: A minimally invasive and reproducible photochemical cortical lesion model for mouse stroke studies. *Journal of Visualized Experiments*, (76), 50370.
- Lee, T. H., Kato, H., Chen, S. T., Kogure, K., & Itoyama, Y. (1998). Expression of nerve growth factor and trkA after transient focal cerebral ischemia in rats. *Stroke*, 29(8), 1687–1696 discussion 1697.
- Liddelov, S. A., Guttenplan, K. A., Clarke, L. E., Bennett, F. C., Bohlen, C. J., Schirmer, L., Bennett, M. L., Münch, A. E., Chung, W. S., Peterson, T. C., Wilton, D. K., Frouin, A., Napier, B. A., Panicker, N., Kumar, M., Buckwalter, M. S., Rowitch, D. H., Dawson, V. L., Dawson, T. M., ... Barres, B. A. (2017). Neurotoxic reactive astrocytes are induced by activated microglia. *Nature*, 541(7638), 481–487. <https://doi.org/10.1038/nature21029>
- Litvinov, R. I., & Weisel, J. W. (2016). What is the biological and clinical relevance of fibrin? *Seminars in Thrombosis and Hemostasis*, 42(4), 333–343. <https://doi.org/10.1055/s-0036-1571342>
- Liu, Z., & Chopp, M. (2016). Astrocytes, therapeutic targets for neuroprotection and neurorestoration in ischemic stroke. *Progress in Neurobiology*, 144, 103–120. <https://doi.org/10.1016/j.pneurobio.2015.09.008>
- Martino, M. M., Briquez, P. S., Ranga, A., Lutolf, M. P., & Hubbell, J. A. (2013). Heparin-binding domain of fibrin(ogen) binds growth factors and promotes tissue repair when incorporated within a synthetic matrix. *Proceedings of the National Academy of Sciences of the United States of America*, 110(12), 4563–4568.
- Nakashima, K., Yanagisawa, M., Arakawa, H., Kimura, N., Hisatsune, T., Kawabata, M., Miyazono, K., & Taga, T. (1999). Synergistic signaling in fetal brain by STAT3-Smad1 complex bridged by p300. *Science*, 284(5413), 479–482. <https://doi.org/10.1126/science.284.5413.479>
- Okada, S., Nakamura, M., Katoh, H., Miyao, T., Shimazaki, T., Ishii, K., Yamane, J., Yoshimura, A., Iwamoto, Y., Toyama, Y., & Okano, H. (2006). Conditional ablation of Stat3 or Socs3 discloses a dual role for reactive astrocytes after spinal cord injury. *Nature Medicine*, 12(7), 829–834.
- O'Shea, T. M., Burda, J. E., & Sofroniew, M. V. (2017). Cell biology of spinal cord injury and repair. *The Journal of Clinical Investigation*, 127(9), 3259–3270. <https://doi.org/10.1172/JCI90608>
- Paul, J., Strickland, S., & Melchor, J. P. (2007). Fibrin deposition accelerates neurovascular damage and neuroinflammation in mouse models of Alzheimer's disease. *The Journal of Experimental Medicine*, 204(8), 1999–2008.
- Pekny, M., Wilhelmsson, U., & Pekna, M. (2014). The dual role of astrocyte activation and reactive gliosis. *Neuroscience Letters*, 565, 30–38. <https://doi.org/10.1016/j.neulet.2013.12.071>
- Petersen, M. A., Ryu, J. K., & Akassoglou, K. (2018). Fibrinogen in neurological diseases: Mechanisms, imaging and therapeutics. *Nature Reviews. Neuroscience*, 19(5), 283–301. <https://doi.org/10.1038/nrn.2018.13>



- Petersen, M. A., Ryu, J. K., Chang, K. J., Etxeberria, A., Bardehle, S., Mendiola, A. S., Kamau-Devers, W., Fancy, S. P. J., Thor, A., Bushong, E. A., Baeza-Raja, B., Syme, C. A., Wu, M. D., Rios Coronado, P. E., Meyer-Franke, A., Yahn, S., Pous, L., Lee, J. K., Schachtrup, C., ... Akassoglou, K. (2017). Fibrinogen activates BMP signaling in oligodendrocyte progenitor cells and inhibits Remyelination after vascular damage. *Neuron*, 96(5), 1003–1012. <https://doi.org/10.1016/j.neuron.2017.10.008>
- Pous, L., Deshpande, S. S., Nath, S., Mezey, S., Malik, S. C., Schildge, S., Bohrer, C., Topp, K., Pfeifer, D., Fernández-Klett, F., Doostkam, S., Galanakis, D. K., Taylor, V., Akassoglou, K., & Schachtrup, C. (2020). Fibrinogen induces neural stem cell differentiation into astrocytes in the subventricular zone via BMP signaling. *Nature Communications*, 11(1), 630. <https://doi.org/10.1038/s41467-020-14466-y>
- Rooney, M. M., Parise, L. V., & Lord, S. T. (1996). Dissecting clot retraction and platelet aggregation. Clot retraction does not require an intact fibrinogen gamma chain C terminus. *The Journal of Biological Chemistry*, 271(15), 8553–8555. <https://doi.org/10.1074/jbc.271.15.8553>
- Ryu, J. K., & McLarnon, J. G. (2009). A leaky blood-brain barrier, fibrinogen infiltration and microglial reactivity in inflamed Alzheimer's disease brain. *Journal of Cellular and Molecular Medicine*, 13(9A), 2911–2925. <https://doi.org/10.1111/j.1582-4934.2008.00434.x>
- Ryu, J. K., Rafalski, V. A., Meyer-Franke, A., Adams, R. A., Poda, S. B., Rios Coronado, P. E., Pedersen, L. Ø., Menon, V., Baeten, K. M., Sikorski, S. L., Bedard, C., Hanspers, K., Bardehle, S., Mendiola, A. S., Davalos, D., Machado, M. R., Chan, J. P., Plastira, I., Petersen, M. A., ... Akassoglou, K. (2018). Fibrin-targeting immunotherapy protects against neuroinflammation and neurodegeneration. *Nature Immunology*, 19(11), 1212–1223. <https://doi.org/10.1038/s41590-018-0232-x>
- Schachtrup, C., Le Moan, N., Passino, M. A., & Akassoglou, K. (2011). Hepatic stellate cells and astrocytes: Stars of scar formation and tissue repair. *Cell Cycle*, 10(11), 1764–1771.
- Schachtrup, C., Lu, P., Jones, L. L., Lee, J. K., Lu, J., Sachs, B. D., Zheng, B., & Akassoglou, K. (2007). Fibrinogen inhibits neurite outgrowth via beta 3 integrin-mediated phosphorylation of the EGF receptor. *Proceedings of the National Academy of Sciences of the United States of America*, 104(28), 11814–11819.
- Schachtrup, C., Ryu, J. K., Helmrick, M. J., Vagena, E., Galanakis, D. K., Degen, J. L., Margolis, R. U., & Akassoglou, K. (2010). Fibrinogen triggers astrocyte scar formation by promoting the availability of active TGF-beta after vascular damage. *The Journal of Neuroscience*, 30(17), 5843–5854.
- Schachtrup, C., Ryu, J. K., Mammadzada, K., Khan, A. S., Carlton, P. M., Perez, A., Christian, F., Le Moan, N., Vagena, E., Baeza-Raja, B., Rafalski, V., Chan, J. P., Nitschke, R., Houslay, M. D., Ellisman, M. H., Wyss-Coray, T., Palop, J. J., & Akassoglou, K. (2015). Nuclear pore complex remodeling by p75 cleavage controls TGF-beta signaling and astrocyte functions. *Nature Neuroscience*, 18(8), 1077–1080.
- Schildge, S., Bohrer, C., Beck, K., & Schachtrup, C. (2013). Isolation and culture of mouse cortical astrocytes. *Journal of Visualized Experiments*, (71), 50079. <https://doi.org/10.3791/50079>
- Silver, J., & Miller, J. H. (2004). Regeneration beyond the glial scar. *Nature Reviews. Neuroscience*, 5(2), 146–156.
- Sofroniew, M. V. (2005). Reactive astrocytes in neural repair and protection. *The Neuroscientist*, 11(5), 400–407.
- Sofroniew, M. V. (2009). Molecular dissection of reactive astrogliosis and glial scar formation. *Trends in Neurosciences*, 32(12), 638–647. <https://doi.org/10.1016/j.tins.2009.08.002>
- Sofroniew, M. V. (2018). Dissecting spinal cord regeneration. *Nature*, 557(7705), 343–350. <https://doi.org/10.1038/s41586-018-0068-4>
- Sofroniew, M. V., & Vinters, H. V. (2010). Astrocytes: Biology and pathology. *Acta Neuropathologica*, 119(1), 7–35. <https://doi.org/10.1007/s00401-009-0619-8>
- Stutzmann, J. M., Mary, V., Wahl, F., Grosjean-Piot, O., Uzan, A., & Pratt, J. (2002). Neuroprotective profile of enoxaparin, a low molecular weight heparin, in in vivo models of cerebral ischemia or traumatic brain injury in rats: A review. *CNS Drug Reviews*, 8(1), 1–30. <https://doi.org/10.1111/j.1527-3458.2002.tb00213.x>
- Wanner, I. B., Anderson, M. A., Song, B., Levine, J., Fernandez, A., Gray-Thompson, Z., Ao, Y., & Sofroniew, M. V. (2013). Glial scar borders are formed by newly proliferated, elongated astrocytes that interact to corral inflammatory and fibrotic cells via STAT3-dependent mechanisms after spinal cord injury. *The Journal of Neuroscience*, 33(31), 12870–12886.
- Wheeler, M. A., Jaronen, M., Covacu, R., Zandee, S. E. J., Scalisi, G., Rothhammer, V., Tjon, E. C., Chao, C. C., Kenison, J. E., Blain, M., Rao, V. T. S., Hewson, P., Barroso, A., Gutiérrez-Vázquez, C., Prat, A., Antel, J.P., Hauser, R., & Quintana, F. J. (2019). Environmental control of astrocyte pathogenic activities in CNS inflammation. *Cell*, 176(3), 581–596. <https://doi.org/10.1016/j.cell.2018.12.012>
- Yao, Y., Chen, Z. L., Norris, E. H., & Strickland, S. (2014). Astrocytic laminin regulates pericyte differentiation and maintains blood brain barrier integrity. *Nature Communications*, 5, 3413. <https://doi.org/10.1038/ncomms4413>
- Zamanian, J. L., Xu, L., Foo, L. C., Nouri, N., Zhou, L., Giffard, R. G., & Barres, B. A. (2012). Genomic analysis of reactive astrogliosis. *The Journal of Neuroscience*, 32(18), 6391–6410. <https://doi.org/10.1523/JNEUROSCI.6221-11.2012>
- Zhou, X., Wahane, S., Friedl, M. S., Kluge, M., Friedel, C. C., Avramopou, K., Zachariou, V., Guo, L., Zhang, B., He, X., Friedel, R. H., & Zou, H. (2020). Microglia and macrophages promote corraling, wound compaction and recovery after spinal cord injury via Plexin-B2. *Nature Neuroscience*, 23(3), 337–350. <https://doi.org/10.1038/s41593-020-0597-7>

## SUPPORTING INFORMATION

Additional supporting information may be found in the online version of the article at the publisher's website.

**How to cite this article:** Conforti, P., Mezey, S., Nath, S., Chu, Y.-H., Malik, S. C., Martínez Santamaría, J. C., Deshpande, S. S., Pous, L., Zieger, B., & Schachtrup, C. (2022). Fibrinogen regulates lesion border-forming reactive astrocyte properties after vascular damage. *Glia*, 1–16. <https://doi.org/10.1002/glia.24166>